INTERNATIONAL JOURNAL FOR NUMERICAL METHODS IN FLUIDS
Int. J. Numer. Meth. Fluids **31**: 1173–1194 (1999)

A BOUNDARY ELEMENT ANALYSIS OF MULTIPLY CONNECTED THREE-DIMENSIONAL CAVITY MIXING FLOW OF POLYMER SOLUTIONS

ROGER E. KHAYAT*

Department of Mechanical and Materials Engineering, Faculty of Engineering Science, The University of Western Ontario, London, Ontario, Canada N6A 5B9

SUMMARY

The emergence of non-linear dynamics in cavity mixing is examined using the boundary element method (BEM). The method is implemented for the simulation of three-dimensional transient creeping flow of Newtonian or linear viscoelastic fluids of the Jeffreys type. A boundary only formulation in the time domain is proposed for viscoelastic flow. Special emphasis is placed on cavity flow involving multiply connected moving domains. The BEM becomes particularly suited for this case, when part of the boundary (stirrer or rotor) is moving, and the remaining outer part (cavity) is at rest. In contrast to conventional volume methods, the BEM is shown to be much easier to implement since the kinematics of the elements bounding the fluid is known (imposed). It is found that, for a simple cavity flow induced by a rotating vane at constant angular velocity, the tractions at the vane tip and cavity face exhibit *non-linear* periodic dynamical behaviour with time for fluids obeying *linear* constitutive equations.

KEY WORDS: boundary element method; cavity flows; polymer solution

1. INTRODUCTION

Mixing flows constitute a class of the moving boundary type that remains relatively unexplored owing to its geometric complexity. Typically, the flow domain separates two boundaries: the outer boundary (cavity), which is stationary, and the inner boundary (translating and/or rotating stirrer), which moves and induces the flow. In addition to the presence of a moving boundary in such problems, the flow involved is unsteady. Typically, the flow becomes periodic after initial transients have died out following the early stages of the process. Periodic behaviour results, obviously from the periodicity in geometry and regularity in the stirring motion. The time a flow takes to reach steady periodic motion is strongly influenced by the inertia and elasticity of the fluid.

For moving boundary problems, the implementation of conventional volume methods, such as the finite element method (FEM), can often be extremely costly given the requirement for domain remeshing at each time step of the procedure, especially for complex three-dimensional flow. Remeshing or mesh refinement is not required when a boundary integral approach, such as the boundary element method (BEM), is used. The BEM mesh is confined to the

* Correspondence to: Department of Mechanical and Materials Engineering, Faculty of Engineering Science, The University of Western Ontario, London, Ontario, Canada N6A 5B9. E-mail: khayat@eng.uwo.ca

CCC 0271–2091/99/231173–22$17.50

Received July 1998
Revised December 1998

boundary(ies) of the flow domain. The BEM offers the obvious advantage when dealing with moving domain problems as it necessitates only the discretization of the boundary and not that of the inner volume domain. The three-dimensional problem is therefore reduced to computing the flow field on the two-dimensional boundary. For example, for the flow inside a cavity induced by the movement of a stirrer; only the (inner) cavity wall together with the (outer) surface of the stirrer need to be discretized.

Modelling of the mixing process has been extensively studied in the transition or turbulent regime [1–4], but less so for the laminar regime, especially of viscoelastic fluids. Chien *et al.* [5] proposed a versatile experimental set-up to generate various low-Reynolds number situations in closed long cavities and to visualize streamlines. In that study, the essentially planar flow was examined, together with the deviation of the velocity component in the direction perpendicular to the plane of the flow. A comparison between photographs taken under different flow conditions and numerical predictions of the FEM results led to an excellent agreement. The efficiency of the mixing process was also assessed according to the dimensionless frequency of oscillation for each flow configuration. Alternate periodic flows were found to be more efficient from the mixing viewpoint than steady flows since they are not always integrable and may lead to the presence of a Smale horseshoe function [6] and chaotic behaviour. More recently, Leong and Ottino [7] studied, in detail, the macroscopic structures of chaotic mixing. The experimental stretching rate was taken as a mixing criterion for several conditions of flow bifurcation, birth and collapse of islands. The lid-driven rectangular-shaped cavity flow problem was investigated by Cortes and Miller [8]. Simulations were carried out using the spectral method for two- and three-dimensional flows for the Laplace and Navier–Stokes equations, with the pressure-correction at Reynolds numbers up to 10000. The algorithm was quite efficient, requiring very modest computing resources for the type of problem investigated.

The mixing of polymer blends was simulated by Graman *et al.* [9] using the BEM for a two-dimensional non-Newtonian flow and advective heat transfer. The convective non-linearities in the energy equation and non-linearities related to the non-Newtonian nature of the flow were treated using the dual-reciprocity BEM, a method proved to be numerically stable. The dynamics of vortex formation in a cavity flow was studied by Gustafson and Halasi [10] for a wide range of Reynolds numbers, from 10^{-6} to 2000, and various aspect ratios. These authors computed unsteady two-dimensional solutions using the finite difference (control volume) method with Euler explicit time stepping. Velocity distributions, pressure gradients as well as the kinetic energy, eddy centres, secondary eddy separations and coalescence were computed and validated against earlier data. Bruneau and Jouron [11] predicted numerically the formation of vortex flow in two-dimensional cavities at higher Reynolds numbers (100–5000), and described the limit conditions for the onset of turbulence. Various numerical techniques were used, consisting of the finite difference method (FDM) with staggered grids for the treatment of the convection terms in the Navier–Stokes equations and the relaxation for all the variables. At still higher Reynolds numbers, the transition to turbulence and bifurcation phenomena in a two-dimensional cavity were predicted to occur; the reader is referred to the works of Goodrich *et al.* [12] and Jie Shen [13] for further details.

The present paper examines a three-dimensional mixing flow induced by the rotation of a stirrer inside a cavity. Although the fluids investigated obey linear constitutive equations, the flow exhibits a rich sequence of non-linear behaviour. The fluids examined are creeping Newtonian and linear viscoelastic of the Oldroyd-B type. A similar non-linear dynamical behaviour is usually expected in the presence of non-linear effects, such as fluid inertia or elasticity (normal stresses that lead to the well-known rod climbing Weissenberg phenomenon).

Using low-dimensional dynamical systems, Khayat [14–19] examined extensively the influence of fluid elasticity on the stability and bifurcation of flows of highly elastic polymeric solutions. These are the well-known Boger fluids, which obey the Oldroyd-B constitutive equation [20]. The studies focused on the emergence of non-linear dynamics in simple flow configurations, such as the flow between two concentric co-rotating cylinders (Taylor–Couette flow) [14,15] and the thermal convection between two parallel plates (Rayleigh–Benard convection) [16–19]. It is found that elasticity precipitates the onset of instability, but tends to regularize the dynamics of the flow in the post-critical range. The validity of the low-dimensional system approach was established by direct comparison with the experiments of Muller *et al.* [21]; excellent agreement was achieved [15]. Although efficient for a simple geometry and highly non-linear fluids, this approach is inadequate for a complex three-dimensional flow. Only linear Newtonian and viscoelastic fluids will be considered in the present study, given the complexity of the flow configuration.

For non-linear viscoelastic problems, the BEM traditionally requires the discretization of a volume integral, which includes all the non-linear terms in the form of a pseudo-body force [22–25]. In this case, the major advantage of the BEM is lost as a result of the inner volume discretization. More recent techniques, such as the methods of dual- and multiple-reciprocity, have been developed to transform the volume integral into a boundary integral [26–29]. Although these methods still require the evaluation of the flow field at internal points, they do not require the discretization of the inner domain, and the BEM retains its primary advantage. However, the capability of such techniques to handle highly non-linear problems, such as flows with strong inertia or (elastic) normal stress effects, remains questionable. The present work will thus be limited to linear viscoelastic flow obeying the Oldroyd-B equation.

Unlike many existing BEM formulations for linear viscoelastic problems in the frequency domain [30–32], the boundary integral equations in the current study are derived and solved in the time domain. The derivation of the boundary integral equation for a viscoelastic flow is based on the Laplace transform of the flow variables. The association of the integral transform of the viscoelastic solution with that associated with the Newtonian flow problem is similar to the correspondence principle for linear viscoelastic solids or the elastico-viscoelastic analogy [32–34]. Although the derivation given here uses the Laplace transform, an analogous procedure follows from the use of the Fourier transform. Read [35] was the first to recognize this association through the Fourier transform, while Sips [36], Brull [37] and Lee [38] gave the corresponding Laplace transform results. The present procedure involves replacing the viscosity with the appropriate form in the transformed equations, and reinterpreting the transformed flow variables as transformed viscoelastic field variables. The transformed equations are then solved and the solution is inverted to obtain the evolution of the flow field with time. In the present work, however, the inversion is avoided and the boundary integral equations are derived in the time domain. A time marching scheme is then implemented for the discretization of the time derivatives and the solution of the integral equations.

2. GOVERNING EQUATIONS, BOUNDARY AND INITIAL CONDITIONS

In this section, the governing equations and boundary conditions are briefly reviewed, together with some of the assumptions adopted in the present study. The governing equations will be discussed for a general flow of an incompressible viscoelastic fluid. The boundary and initial conditions will then be discussed for the flow inside the cavity mixer, which will be analysed in the present study.

2.1. Governing equations

Consider a fluid occupying a three-dimensional region, $\Omega(t)$, that may change with time t. The fluid is assumed to be an incompressible Newtonian or viscoelastic fluid. Inertia and body forces are assumed negligible. The conservation of mass and linear momentum equations are then given by

$$\nabla\cdot\mathbf{u}(\mathbf{x},t)=0, \qquad \nabla\cdot\boldsymbol{\sigma}(\mathbf{x},t)=\mathbf{0}, \quad \mathbf{x}\in\Omega(t)\cup\Gamma(t), \tag{1}$$

where ∇ is the gradient operator, $\mathbf{x}$ is the position vector, $\mathbf{u}(\mathbf{x},t)$ is the velocity vector and $\boldsymbol{\sigma}(\mathbf{x},t)$ is the total stress tensor. The time derivative of the velocity, $(\partial\mathbf{u}/\partial t)$, in the momentum conservation equation is neglected, so that for a Newtonian fluid, the formulation in question is not strictly unsteady, but quasi-steady. This quasi-steady state assumption is valid whenever $L^2/\nu \ll T$, where L and T are typical characteristic length and time of the flow, and ν is the kinematic viscosity. In the present case, $T\sim L/U$, and U is a typical value of the driving velocity. Thus, for the quasi-steady state assumption to apply, one must have the Reynolds number $UL/\nu \ll 1$. Thus, the quasi-steady assumption is equivalent to setting the Reynolds number equal to zero. This is indeed typical of the case for fluids of interest to mixing problems. Physically, the quasi-steady state approximation means that a Newtonian fluid immediately adjusts to changes in the movement of the boundary or boundary conditions. This is not necessarily the case for a viscoelastic fluid.

The fluids examined in the present study are polymer solutions of viscosity μ. It is assumed that the solution is composed of a polymer solute in a Newtonian solvent, with viscosities μ_p and μ_s respectively. In this case, $\mu=\mu_p+\mu_s$. The total stress $\boldsymbol{\sigma}(\mathbf{x},t)$ may then be expressed as a sum of the Newtonian and elastic contributions, such that

$$\boldsymbol{\sigma}(\mathbf{x},t)=-p(\mathbf{x},t)\mathbf{I}+\mu_s\boldsymbol{\gamma}(\mathbf{x},t)+\boldsymbol{\tau}(\mathbf{x},t), \tag{2}$$

where $p(\mathbf{x},t)$ is the hydrostatic pressure, $\boldsymbol{\tau}(\mathbf{x},t)$ is the elastic part of the stress tensor, μ is the viscosity of the fluid, $\boldsymbol{\gamma}(\mathbf{x},t)\equiv\nabla\mathbf{u}(\mathbf{x},t)+\nabla\mathbf{u}^t(\mathbf{x},t)$ is the rate-of-strain tensor, and $\mathbf{I}$ is the identity tensor. Let $\mathbf{T}(\mathbf{x},t)$ be the excess stress tensor, defined by

$$\mathbf{T}(\mathbf{x},t)=\mu_s\boldsymbol{\gamma}(\mathbf{x},t)+\boldsymbol{\tau}(\mathbf{x},t). \tag{3}$$

Next, a suitable constitutive equation for $\mathbf{T}(\mathbf{x},t)$ is selected.

Generally, the flow is expected to be influenced significantly by the constitutive model. This is typically the case when non-linear effects, such as shear thinning and normal stresses, are accounted for in the model. However, in the linear range of flow, most constitutive equations reduce to Maxwell's model or one of its variants [20]. Thus, the flow behaviour of linear fluids is not expected to depend on the constitutive model. For this reason, the choice of a model is not critical in the present study. The study's major objective is to investigate the influence of fluid elasticity on an already complex (mixing) flow as it arises for Newtonian fluids alone. It is then more prudent to adopt as simple a viscoelastic constitutive equation as possible. However, the assumption of a linear constitutive behaviour makes the approach inadequate to handle highly non-linear viscoelastic phenomena. Thus, although large strains are present in the flows examined here, only small strain rates are assumed to be involved, making the usually important non-linearities in the constitutive equation negligible. Such non-linearities typically stem from convective and upper-convective terms, the dependence of viscosity and relaxation time on the rate-of-strain tensor. Since elastic effects are the main focus in this study, elastic non-linearities (normal stresses that lead to the Weissenberg rod-climbing phenomenon) can be quantified by ensuring that the value of the Deborah number, De, is small. Thus, the ratio of the relaxation time of the fluid to a typical hydrodynamic time of the flow is assumed to be small [20].

Although Maxwell's equation is the simplest constitutive model, it is not suitable for polymeric solutions. In this study, the simplest constitutive equation for $\mathbf{T}$ is taken to correspond to the Jeffreys model [20]

$$\lambda_1\dot{\mathbf{T}}(\mathbf{x}, t) + \mathbf{T}(\mathbf{x}, t) = \mu[\gamma(\mathbf{x}, t) + \lambda_2\dot{\gamma}(\mathbf{x}, t)], \quad \mathbf{x}\in\Omega(t)\cup\Gamma(t), \tag{4}$$

where λ_1 and λ_2 $(0 \le \lambda_2 \le \lambda_1)$ are two constants, the relaxation and the retardation times of the fluid respectively. An overdot denotes partial differentiation with respect to time. The equations governing $\mathbf{u}(\mathbf{x}, t)$, $p(\mathbf{x}, t)$ and $\boldsymbol{\tau}(\mathbf{x}, t)$ follow from Equations (1)–(4), and may be written here as

$$\nabla\cdot\mathbf{u}(\mathbf{x}, t) = 0, \tag{5}$$

$$\nabla\cdot\boldsymbol{\tau}(\mathbf{x}, t) + \mu_s\nabla^2\mathbf{u}(\mathbf{x}, t) - \nabla p(\mathbf{x}, t) = \mathbf{0}, \quad \mathbf{x}\in\Omega(t)\cup\Gamma(t), \tag{6}$$

$$\lambda_1\dot{\boldsymbol{\tau}}(\mathbf{x}, t) + \boldsymbol{\tau}(\mathbf{x}, t) = \mu_p\gamma(\mathbf{x}, t). \tag{7}$$

Note that, in this case, the retardation time is related to the relaxation time and the polymer-to-solvent viscosity ratio:

$$\lambda_2 = \frac{\lambda_1}{1 + \dfrac{\mu_p}{\mu_s}} = \frac{\mu_s\lambda_1}{\mu}. \tag{8}$$

In the limit $\mu_s \to 0$, Equations (6) and (7) reduce to the equations corresponding to Maxwell flow or polymer melt. The Newtonian limit is recovered if, further, $\lambda_1 \to 0$.

2.2. Boundary and initial conditions

The geometry of the cavity mixer considered in this study is shown in Figure 1. It is emphasized that the current formulation and solution method can handle other more complex

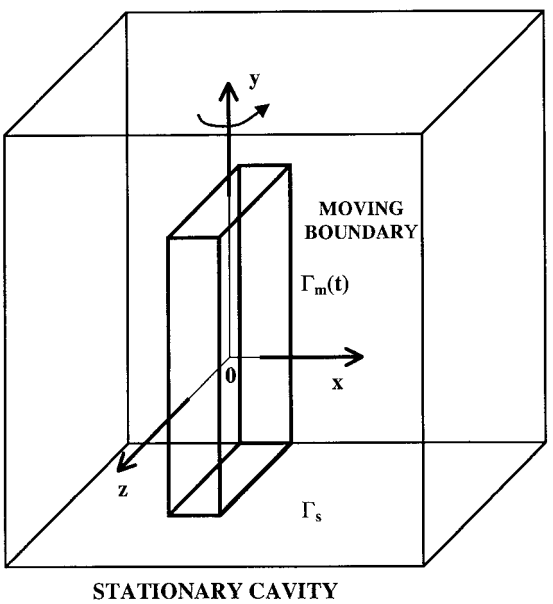

Figure 1. Schematic view of a mixing flow inside a cavity with a rotating vane in a cubic cavity of unit side. The figure illustrates the co-ordinate system and the initial position of the vane.

flows with moving boundary(ies). Typically, the velocity is prescribed on the moving part of the boundary, $\Gamma_m(t)$, and the velocity or the traction is imposed on the remaining stationary part Γ_s. In this case, $\Gamma(t) = \Gamma_s \cup \Gamma_m(t)$ is the boundary surrounding $\Omega(t)$, with Γ_s being stationary and $\Gamma_m(t)$ undergoing rigid body rotation. The flow is thus induced by the movement of $\Gamma_m(t)$ and/or by the imposed velocity or traction on Γ_s. In the present work, the velocity is always prescribed on $\Gamma_m(t)$, so that

$$\mathbf{u}(\mathbf{x}, t) = \mathbf{u}_m(t), \quad \mathbf{x} \in \Gamma_m(t), \tag{9a}$$

and either the velocity or the traction is imposed on the stationary part,

$$\mathbf{u}(\mathbf{x}, t) = \mathbf{u}_s(t) \quad \text{or} \quad \mathbf{t}(\mathbf{x}, t) = \mathbf{t}_s(t), \quad \mathbf{x} \in \Gamma_s, \tag{9b}$$

where the traction is defined as $\mathbf{t}(\mathbf{x}, t) \equiv \boldsymbol{\sigma}(\mathbf{x}, t) \cdot \mathbf{n}(\mathbf{x}, t)$, $\mathbf{n}(\mathbf{x}, t)$ being the unit normal vector at the boundary, pointing away from $\Omega(t)$. As to the initial conditions, the fluid is assumed to be at rest initially; the fluid is in a stress free state:

$$\mathbf{u}(\mathbf{x}, t = 0) \equiv \mathbf{0}, \qquad \mathbf{t}(\mathbf{x}, t = 0) = \mathbf{0}, \quad \mathbf{x} \in \Omega(t = 0) \cup \Gamma(t = 0). \tag{10}$$

The assumption of initial equilibrium may seem incompatible with the assumption that the acceleration term in the momentum equation is negligible. This is certainly true if the initial jump in the boundary condition(s) is significant. However, since the viscosity of the fluid and the imposed velocity are typically low, the assumption of negligible acceleration, even initially, may still be valid. Conditions (10) greatly simplify the solution procedure for the viscoelastic flow as will be seen below.

3. PROBLEM FORMULATION FOR A MOVING DOMAIN

In this section, the boundary integral equation is derived for the general viscoelastic flow problem, and its numerical implementation is carried out in the context of mixing flow. The numerical solution procedure and time marching scheme are also described. While the formalism behind the BEM for Stokes flow is well established [39–41], that corresponding to viscoelastic fluids is relatively unexplored. Given the linearity of the constitutive equation (4), the governing equations can be Laplace transformed. The problem reduces to that corresponding to Stokes flow in the frequency domain. The Voltera principle in the frequency domain, which is also known as the correspondence principle [32–34], allows the solution of a boundary value problem in viscoelasticity to be obtained from the solution of the corresponding Newtonian problem, with the viscosity being replaced by a transformed characteristic of the fluid. The final boundary integral equation is obtained in the time domain.

3.1. Generalized boundary integral equation for a viscoelastic fluid

The first step in the procedure consists of taking the Laplace transform of the governing equations (5)–(7). Since the fluid is incompressible, and inertia is neglected, the transformed continuity and momentum equations retain the same form in the frequency domain

$$\nabla \cdot \bar{\mathbf{u}}(\mathbf{x}, s) = 0, \tag{11}$$

$$\nabla \cdot \bar{\boldsymbol{\tau}}(\mathbf{x}, s) + \mu_s \nabla^2 \bar{\mathbf{u}}(\mathbf{x}, s) - \nabla \bar{p}(\mathbf{x}, s) = 0, \quad \mathbf{x} \in \Omega(t) \cup \Gamma(t), \tag{12}$$

where an overbar on the velocity or stress variable designates Laplace transformation. Note that the parameter s should be viewed as a constant, and the (transformed) variables by $\bar{\mathbf{u}}(\mathbf{x}, s)$, $\bar{p}(\mathbf{x}, s)$ and $\bar{\boldsymbol{\tau}}(\mathbf{x}, s)$ represent a (transformed) flow in the original domain, $\Omega(t) \cup \Gamma(t)$. An expression for the transformed excess stress is also obtained from Equation (7) in terms of the transformed rate-of-strain tensor, which is mathematically equivalent to Newton's law of viscosity

$$\bar{\boldsymbol{\tau}}(\mathbf{x}, s) = \bar{\mu}[\nabla\bar{\mathbf{u}}(\mathbf{x}, s) + \nabla\bar{\mathbf{u}}^t(\mathbf{x}, s)]. \tag{13}$$

If Equation (13) is inserted into Equation (12), and Equation (11) is used, then the momentum equation in the frequency domain takes the same form as for Stokes flow, i.e.

$$\bar{\mu}\nabla^2\bar{\mathbf{u}}(\mathbf{x}, s) - \nabla\bar{p}(\mathbf{x}, s) = \mathbf{0}, \quad \bar{\mu} = \left(\frac{\lambda_2 s + 1}{\lambda_1 s + 1}\right)\mu. \tag{14}$$

Note that an equivalent viscosity, $\bar{\mu}$, is now obtained, which is a function of the Laplace parameter s. The problem is now solved similarly to the flow of a Newtonian fluid, with s taken as a constant parameter.

In order to derive the integral representation for Equations (11) and (14), the fundamental solution for the problem is needed. For a Newtonian fluid, this singular solution corresponds to the velocity and stress fields at a point $\mathbf{x}$ produced by a point force $\bar{\mathbf{F}}(s)\delta(\mathbf{x} - \mathbf{y})$ located at $\mathbf{y}$. In this case, the acting force is generally a function of the parameter s, and therefore depends on time. For a viscoelastic fluid, this also corresponds to the same force that starts to act initially at time $t = 0$. In other words, the force in real time is given by $\mathbf{F}\delta(\mathbf{x} - \mathbf{y})\delta(t)$, where δ is the Dirac delta function. Denoting the singular solution with asterisks, and taking the Laplace transform of the viscoelastic equations over the infinite medium, the problem reduces to that corresponding to Stokes flow in the frequency domain

$$\nabla\cdot\bar{\mathbf{u}}^*(\mathbf{x}|\mathbf{y}, s) = 0, \qquad \nabla\cdot\bar{\boldsymbol{\sigma}}^*(\mathbf{x}|\mathbf{y}, s) = \bar{\mathbf{F}}(s)\delta(\mathbf{x} - \mathbf{y}), \tag{15a}$$

with the following boundary conditions:

$$|\bar{\mathbf{u}}^*(\mathbf{x}|\mathbf{y}, s)| \to 0, \qquad |\bar{\boldsymbol{\sigma}}^*(\mathbf{x}|\mathbf{y}, s)| \to 0, \qquad |\mathbf{x}| \to \infty. \tag{15b}$$

This yields the following expressions for the transformed velocity $\bar{\mathbf{u}}^*(\mathbf{x}|\mathbf{y}, s)$ and stress $\bar{\boldsymbol{\sigma}}^*(\mathbf{x}|\mathbf{y}, s)$, namely,

$$\bar{\mathbf{u}}^*(\mathbf{x}|\mathbf{y}, s) = \left(\frac{\lambda_1 s + 1}{\lambda_2 s + 1}\right)\mathbf{J}(\mathbf{x}|\mathbf{y})\cdot\bar{\mathbf{F}}(s), \qquad \bar{\boldsymbol{\sigma}}^*(\mathbf{x}|\mathbf{y}, s) = \mathbf{K}(\mathbf{x}|\mathbf{y})\cdot\bar{\mathbf{F}}(s). \tag{16}$$

The kernels, or Green's functions, $\mathbf{J}$ and $\mathbf{K}$ are second and third rank tensors respectively, and are given by

$$\mathbf{J}(\mathbf{x}|\mathbf{y}) = \frac{1}{8\pi\mu}\left(\frac{\mathbf{I}}{r} - \frac{\mathbf{rr}}{r^3}\right), \qquad \mathbf{K}(\mathbf{x}|\mathbf{y}) = \frac{3}{4\pi}\frac{\mathbf{rrr}}{r^5}, \tag{17}$$

for an unbounded three-dimensional domain, where $\mathbf{r} = \mathbf{x} - \mathbf{y}$ and $r = |\mathbf{x} - \mathbf{y}|$. Note that $\mathbf{J}$ and $\mathbf{K}$ are respectively symmetric and anti-symmetric tensors with respect to $\mathbf{r}$. The corresponding integral representation is now derived similar to that corresponding to Stokes flow. The Reciprocal (Green's) theorem is first invoked, relating the fields $(\bar{\mathbf{u}}, \bar{\boldsymbol{\sigma}})$ and $(\bar{\mathbf{u}}^*, \bar{\boldsymbol{\sigma}}^*)$. The theorem is straightforward to derive [39–41] and its statement for the present problem is as follows:

$$\int_{\Omega(t)} \{\bar{\mathbf{u}}(\mathbf{y}, s)\cdot[\nabla_{\mathbf{y}}\cdot\bar{\boldsymbol{\sigma}}^*(\mathbf{x}|\mathbf{y}, s)] - \bar{\mathbf{u}}^*(\mathbf{x}|\mathbf{y}, s)\cdot[\nabla_{\mathbf{y}}\cdot\bar{\boldsymbol{\sigma}}(\mathbf{y}, s)]\}\, d\Omega_{\mathbf{y}}$$
$$= \int_{\Gamma(t)} \mathbf{n}(\mathbf{y}, t)\cdot[\bar{\boldsymbol{\sigma}}^*(\mathbf{x}|\mathbf{y}, s)\cdot\bar{\mathbf{u}}(\mathbf{y}, s) - \bar{\boldsymbol{\sigma}}(\mathbf{y}, s)\cdot\bar{\mathbf{u}}^*(\mathbf{x}|\mathbf{y}, s)]\, d\Gamma_{\mathbf{y}}, \tag{18}$$

where it is noted that $\mathbf{n}(\mathbf{y}, t)$, which is the normal to and pointing away from $\Gamma(t)$, is time-dependent for a moving domain. Substitution of the fundamental singular solution (16) into theorem (18), using (1), removing the arbitrary vector $\bar{\mathbf{F}}$, and interchanging the labelled $\mathbf{x}$ and $\mathbf{y}$, lead to the following integral equation in the frequency domain:

$$\int_{\Gamma(t)} \mathbf{n}(\mathbf{y}, t)\cdot\left[\left(\frac{\lambda_1 s+1}{\lambda_2 s+1}\right)\bar{\boldsymbol{\sigma}}(\mathbf{y}, s)\cdot\mathbf{J}(\mathbf{x}|\mathbf{y})\right] d\Gamma_{\mathbf{y}} - \int_{\Gamma(t)} \mathbf{n}(\mathbf{y}, t)\cdot[\bar{\mathbf{u}}(\mathbf{y}, s)\cdot\mathbf{K}(\mathbf{x}|\mathbf{y})]\, d\Gamma_{\mathbf{y}}$$
$$= c(\mathbf{x}, t)\bar{\mathbf{u}}(\mathbf{x}, s), \quad \mathbf{x}\in\Omega(t)\cup\Gamma(t), \tag{19}$$

where $c(\mathbf{x}, t)$ is equal to 1 for $\mathbf{x}$ belonging to the interior of $\Omega(t)$, and for a point on the boundary $\Gamma(t)$, its value depends on the jump in the value of the first integral on the boundary as the boundary is crossed. Thus, $c(\mathbf{x}, t) = \frac{1}{2}$ if the boundary is Lyapunov smooth, which requires that a local tangent to the boundary exists everywhere. This assumption, however, is not valid in the vicinity of sharp corners, cusps or edges. In such cases, a separate treatment is needed.

The inverse Laplace transform of Equation (19) is taken to obtain the desired integral equation in the time domain. It is not difficult to see that the Laplace inversion of Equation (19) leads to the following time-dependent integral equation:

$$\int_{\Gamma(t)} \mathbf{n}(\mathbf{y}, t)\cdot\left[\lambda_1\frac{\partial\boldsymbol{\sigma}(\mathbf{y}, t)}{\partial t} + \boldsymbol{\sigma}(\mathbf{y}, t)\right]\cdot\mathbf{J}(\mathbf{x}|\mathbf{y})\, d\Gamma_{\mathbf{y}}$$
$$- \int_{\Gamma(t)} \mathbf{n}(\mathbf{y}, t)\cdot\left[\lambda_2\frac{\partial\mathbf{u}(\mathbf{y}, t)}{\partial t} + \mathbf{u}(\mathbf{y}, t)\right]\cdot\mathbf{K}(\mathbf{x}|\mathbf{y})\, d\Gamma_{\mathbf{y}} = c(\mathbf{x}, t)\left[\lambda_2\frac{\partial\mathbf{u}(\mathbf{x}, t)}{\partial t} + \mathbf{u}(\mathbf{x}, t)\right], \tag{20}$$

for the class of problems envisaged in the present study.

In the derivation of Equation (20), the fluid is tacitly assumed to be in a state of rest initially, or more particularly, in a stress-free state. As mentioned earlier, this assumption greatly simplifies the formulation. Indeed, the inclusion of an initial stress condition leads to an additional term in Equation (13) when the Laplace transform of the constitutive equation (2) is taken. If the initial stress is not generally a constant, thus is dependent on position, a volume integral emerges, which must be added to the integral equation (19) in the frequency domain. Correspondingly, a volume integral emerges in Equation (20) in the time domain. It is obvious that the presence of a volume integral complicates matters significantly, and may not be necessary for a wide range of practical flow problems.

3.2. Limit cases

If the fluid is a polymer melt rather than a polymer solution, then $\lambda_2 \to 0$, and Equation (2) reduces to the Maxwell constitutive model. The corresponding integral equation for a Maxwell fluid is obtained by taking [equivalently from Equation (8)] the limit $\mu_2 \to 0$ in Equation (20),

$$\int_{\Gamma(t)} \mathbf{n}(\mathbf{y}, t)\cdot\left[\lambda_1\frac{\partial\boldsymbol{\sigma}(\mathbf{y}, t)}{\partial t} + \boldsymbol{\sigma}(\mathbf{y}, t)\right]\cdot\mathbf{J}(\mathbf{x}|\mathbf{y})\, d\Gamma_{\mathbf{y}} - \int_{\Gamma(t)} \mathbf{n}(\mathbf{y}, t)\cdot\mathbf{u}(\mathbf{y}, t)\cdot\mathbf{K}(\mathbf{x}|\mathbf{y})\, d\Gamma_{\mathbf{y}}$$
$$= c(\mathbf{x}, t)\mathbf{u}(\mathbf{x}, t), \quad \mathbf{x}\in\Omega(t)\cup\Gamma(t), \tag{21}$$

In addition, in the limit $\lambda_1 \to 0$, Eqaution (21) reduces to the integral equation corresponding to Stokes flow

$$\int_{\Gamma(t)} \mathbf{t}(\mathbf{y}, t)\cdot\mathbf{J}(\mathbf{x}|\mathbf{y})\, d\Gamma_{\mathbf{y}} - \int_{\Gamma(t)} \mathbf{n}(\mathbf{y}, t)\cdot\mathbf{u}(\mathbf{y}, t)\cdot\mathbf{K}(\mathbf{x}|\mathbf{y})\, d\Gamma_{\mathbf{y}} = c(\mathbf{x}, t)\mathbf{u}(\mathbf{x}, t), \quad \mathbf{x}\in\Omega(t)\cup\Gamma(t), \tag{22}$$

Unlike Equations (19) or (20), Equation (22) relates directly the velocity field, $\mathbf{u}(\mathbf{x}, t)$, at any point inside the fluid region, $\Omega(t)$, or on the boundary, $\Gamma(t)$, to the traction, $\mathbf{t}(\mathbf{x}, t)$. The situation is quite different for the viscoelastic flow problem.

The major difficulty in dealing with the solution of Equation (20) is the explicit presence of the stress tensor rather than the traction vector, as in Equation (22). Equation (20) is valid for the general transient viscoelastic flow with moving boundary, where the normal to the boundary changes with time. A direct relation between velocity and traction is not possible unless the normal vector is constant with time. If the domain occupied by the fluid is fixed, $\Gamma(t) = \Gamma$, then the traction may be directly related to the velocity as for Stokes flow. In this case, Equation (20) reduces to

$$\int_{\Gamma}\left[\lambda_1\frac{\partial\mathbf{t}(\mathbf{y}, t)}{\partial t} + \mathbf{t}(\mathbf{y}, t)\right]\cdot\mathbf{J}(\mathbf{x}|\mathbf{y})\, d\Gamma_{\mathbf{y}} - \int_{\Gamma}\mathbf{n}(\mathbf{y})\cdot\left[\lambda_2\frac{\partial\mathbf{u}(\mathbf{y}, t)}{\partial t} + \mathbf{u}(\mathbf{y}, t)\right]\cdot\mathbf{K}(\mathbf{x}|\mathbf{y})\, d\Gamma_{\mathbf{y}}$$
$$= c(\mathbf{x})\left[\lambda_2\frac{\partial\mathbf{u}(\mathbf{x}, t)}{\partial t} + \mathbf{u}(\mathbf{x}, t)\right], \quad \mathbf{x}\in\Omega\cup\Gamma. \tag{23}$$

Note that the flow field may still be time-dependent even though the domain does not change with time. Additional simplifications to Equation (20) may be made in other limit flow cases of relevance to the present problem.

4. NUMERICAL IMPLEMENTATION AND SOLUTION PROCEDURE

The solution of Equation (20) for a general class of cavity mixing problems is first discussed, and then applied to the present problem. A time marching scheme is implemented to discretize the time derivatives in stress (traction) and velocity. The numerical solution of the resulting (discretized) integral equation(s) turns out to be similar to that corresponding to Stokes flow.

4.1. Integral equation for cavity mixing

Consider again cavity mixing, which is typically illustrated in Figure 1. It is assumed that the velocity is always imposed on the stationary and moving boundaries Γ_s and $\Gamma_m(t)$ respectively. In this case, $\Gamma(t) = \Gamma_s\cup\Gamma_m(t)$. On Γ_s, stick conditions apply so that the velocity is zero and Equation (9b) leads to $\mathbf{u}_s(t) = \mathbf{0}$, $\forall t$. But if $\mathbf{u}_s(t)$ vanishes, so does its (time) derivative. Similarly, both $\mathbf{u}_m(t)$ and its derivative are specified on $\Gamma_m(t)$. Since the velocity is completely specified on the boundaries, then Equation (20) will be solved to give the stress or traction on $\Gamma(t)$. It is convenient to introduce generalized traction and velocity as

$$\mathbf{P}(\mathbf{x}, t) = \mathbf{n}(\mathbf{x}, t)\cdot\left[\lambda_1\frac{\partial\boldsymbol{\sigma}(\mathbf{x}, t)}{\partial t} + \boldsymbol{\sigma}(\mathbf{x}, t)\right],$$
$$\mathbf{U}(\mathbf{x}, t) = \lambda_2\frac{\partial\mathbf{u}(\mathbf{x}, t)}{\partial t} + \mathbf{u}(\mathbf{x}, t), \tag{24}$$

so that Equation (20) reduces to

$$\int_{\Gamma_s \cup \Gamma_m(t)} \mathbf{P}(\mathbf{y}, t)\cdot\mathbf{J}(\mathbf{x}|\mathbf{y})\, d\Gamma_y - \int_{\Gamma_m(t)} \mathbf{n}(\mathbf{y}, t)\cdot\mathbf{U}_m(\mathbf{y}, t)\cdot\mathbf{K}(\mathbf{x}|\mathbf{y})\, d\Gamma_y = c(\mathbf{x}, t)\begin{cases}\mathbf{0}, & \mathbf{x}\in\Omega(t)\cup\Gamma_s \\ \mathbf{U}_m(\mathbf{x}, t), & \mathbf{x}\in\Omega(t)\cup\Gamma_m(t)\end{cases}. \tag{25}$$

Consider now the evaluation of $c(\mathbf{x}, t)$ for $\mathbf{x}$ belonging to $\Gamma(t) = \Gamma_s \cup \Gamma_m(t)$. At each time step, t, the value of $c(\mathbf{x}, t)$ depends solely on the geometry of the boundary involved. Thus, $c(\mathbf{x}, t) = \frac{1}{2}$ for a smooth boundary. More generally, if a uniform velocity field is applied over the domain $\Omega(t)\cup\Gamma(t)$, such that $\mathbf{u}(\mathbf{x}, t) = u\mathbf{e}$, where u is the constant magnitude of the velocity and $\mathbf{e}$ is the direction of the flow, then all derivatives (including tractions and stresses) must vanish. Hence, at any time t, Equation (25) reduces to

$$c(\mathbf{x}, t) = \mathbf{ee}\colon \int_{\Gamma(t)} \mathbf{n}(\mathbf{y}, t)\cdot\mathbf{K}(\mathbf{x}|\mathbf{y})\, d\Gamma_y, \quad \mathbf{x}\in\Gamma(t). \tag{26}$$

Equation (25) is a Fredholm integral of the second kind, with $\mathbf{P}(\mathbf{x}, t)$ being the unknown. However, the traction at the boundary is yet to be determined since it is the variable of primary interest in the present study.

4.2. Time marching scheme

Once $\mathbf{P}(\mathbf{x}, t)$ is determined from Equation (25), the time derivative of the stress tensor is approximated by finite difference. The Euler scheme is used and higher-order terms in the time increment Δt are neglected:

$$\mathbf{P}(\mathbf{x}, t) = \mathbf{n}(\mathbf{x}, t)\cdot\left[\lambda_1 \frac{\partial\boldsymbol{\sigma}(\mathbf{x}, t)}{\partial t} + \boldsymbol{\sigma}(\mathbf{x}, t)\right] \approx \left(\frac{\lambda_1}{\Delta t} + 1\right)\mathbf{t}(\mathbf{x}, t) - \frac{1}{\Delta t}\,\mathbf{n}(\mathbf{x}, t)\cdot\boldsymbol{\sigma}(\mathbf{x}, t - \Delta t) + O(\Delta t). \tag{27}$$

This discretization, however, does not yet give $\mathbf{t}(\mathbf{x}, t)$ at the boundary, which is the quantity of primary interest here, unless $\boldsymbol{\sigma}(\mathbf{x}, t - \Delta t)$ is known. The stress at the previous time step can be determined from an additional integral equation that can be derived from Equation (25) similar to Stokes flow [42]. However, a further approximation is used, which greatly simplifies the numerical computation; the normal vector at the current time is expanded around the previous time step. Only the leading term in the Taylor expansion of the normal vector is kept, such that $\mathbf{n}(\mathbf{x}, t)\cdot\boldsymbol{\sigma}(\mathbf{x}, t - \Delta t) \approx \mathbf{t}(\mathbf{x}, t - \Delta t) + O(\Delta t)$, and Equation (27) is reduced, leading to the expression for the current traction:

$$\mathbf{t}(\mathbf{x}, t) \approx \frac{\Delta t\,\mathbf{P}(\mathbf{x}, t) + \mathbf{t}(\mathbf{x}, t - \Delta t)}{\lambda_1 + \Delta t} + O(\Delta t). \tag{28}$$

This approximate expression is of course accurate as long as the time increment, Δt, is small.

4.3. Solution procedure

The current formulation and its computer implementation are intended for typical mixing problems. The geometry involved is usually complex and three-dimensional. Typically, a mixing process involves the motion of part of the boundary, such as in lid-driven cavity flow, or the presence of a second moving boundary, such as a rotor or a stirrer (Figure 1). It is obvious that the BEM becomes particularly advantageous over domain methods in the

presence of a moving obstacle because the computational domain evolves with time. A conventional domain method, such as the FEM, generally necessitates a continuous remeshing of the inner domain; for example, the volume domain located between the rotor and the cavity needs remeshing, although for some problems the volume meshing can be constant as mentioned in Section 1. The BEM requires the discretization of the rigid boundaries only. The discretization of the moving boundary (rotor) does not pose any difficulty. The kinematics of each of the discretization elements is known (imposed) given the boundary is undergoing rigid body motion. In the present work, the motion of the moving boundary is always known so the velocity will be prescribed on $\Gamma_m(t)$.

Equation (25) may be solved using constant or higher-order elements. In this study, the simplest form of the BEM is adopted, and the boundary is discretized into a finite number of constant triangular elements. The velocity and traction are thus assumed to be constant over each surface element and equal to the values at the centroid. In this case, since there are no corner nodes on which the unknown variables are evaluated, the value of $c(\mathbf{x}, t) = \frac{1}{2}$. The resulting discretized equations represent a set of linear algebraic equations in the velocity and traction at the boundary once the integrals are evaluated over each element. The evaluation of the integrals is carried out numerically using Gauss quadrature formulae in the absence of singularities. Since the kernels $\mathbf{J}$ and $\mathbf{K}$ have integrable singularity at $\mathbf{x} = \mathbf{y}$, some care must be taken in the numerical evaluation of the singular integrals. Common procedures either cut out a region surrounding the singularity and perform the integration analytically, or subtract the singularity directly in the numerical approximation of the integral. In the case of constant elements, the analytical evaluation of the singular integrals is straightforward in two dimensions. For the present three-dimensional flow, the singular integrals can also be evaluated analytically through the Cauchy Principle Value theorem [42]. The resulting system of linear equations is solved using the lower–upper (LU) factorization method.

5. RESULTS AND DISCUSSION

In this section the solution of Equation (25) is presented for transient three-dimensional flows of Newtonian and viscoelastic fluids. The accuracy and convergence of the code are first discussed. The time-dependent behaviour of the traction at the cavity wall and rotor of the mixer is monitored with time for different fluids.

5.1. Assessment of convergence and accuracy

The accuracy and CPU requirement of the method were assessed by comparing results based on the BEM with those based on the FEM using the commercial code POLYFLOW™. The comparison was primarily conducted for the solution of Equation (25). All computations were carried out on an IBM (RISK) 590 machine with a speed of 130 MFLOPS (Linpack). The swapping in this case is minimal or non-existent. The computation domain corresponds to a cubic cavity of unit side length, given by $(x, y, z) \in [0, 1]$. The face $y = 1$ is assumed to move at a velocity (1, 0, 0). All dimensions are relative. Stick conditions are imposed on all faces except at the side $z = 1$, which is assumed to be lubricated (or a plane of symmetry). On this side, the velocity distributions based on the BEM and FEM are compared. In this case, the three velocity components (u_x, u_y, u_z) vanish on all faces except at the face $z = 1$, where $u_z = 0$ and $t_x = t_y = 0$.

Most flow activity was concentrated around the edges of the cubic cavity. The symmetry of the flow field with respect to the plane $x = 0.5$ was preserved, reflecting the robustness of the solution procedure. Three FEM mesh sizes were used, corresponding to a total number of

internal and external nodes $N = 64$, 216 and 729, and five BEM meshes corresponding also to a total number of internal and external nodes $N \in [216, 1134]$. Note that the internal nodes in the case of the BEM are not used in the computation but are mentioned here for clarity. In fact, the comparison is meaningful only if the total number of nodes for both methods is comparable. It is understood that although the number of degrees of freedom, corresponding to a given mesh size, can be relatively much smaller for the BEM than for the FEM, the resulting discretized algebraic system is full in the former case and sparse in the latter. Thus, it is difficult *a priori* to anticipate which of the two methods is more advantageous regarding space and time requirement.

The flow field was monitored in the plane of symmetry ($z = 1$), which follows closed streamlines. The location of the field centre depends on the mesh size taken in the computation, and is taken here as a measure for convergence. Regardless of the mesh size used, the centre is always located at $x = \frac{1}{2}$, reflecting the robustness of the method. The height of the centre depends strongly on mesh size. This dependence is reported in Table I. Convergence for the FEM is reasonably achieved between the second and third meshes. The FEM results are accurate only for the finest mesh ($N = 729$) used when compared with the BEM results. The calculation based on a finer FEM mesh was also attempted, but storage problems were encountered. Calculations based on the BEM indicate that convergence is relatively faster. The three finest BEM meshes ($N = 720$, 990 and 1134) lead essentially to the same results (within 1.4% error), and may then be regarded as the exact solution to the problem. This convergence is also confirmed from the trend based on the FEM solutions. Comparison between the FEM with $N = 729$ and the BEM with $N = 720$ tends to confirm, in turn, the general observation that the BEM is more accurate than the FEM since the solution has already converged in this case. This observation is usually well established for two-dimensional problems.

The (absolute) CPU required for each case and method studied was also monitored. The FEM appears to be more time consuming than the BEM when the same number of nodes is used. It is clear from the two curves in the figure that the CPU requirement tends to grow much faster for the FEM ($\sim N^{2.36}$) than for the BEM ($\sim N^{1.2}$). Although these comparisons appear to be conclusive, they should not be regarded as so. First, on the one hand, additional calculations must be carried out involving a geometry other than that of a cube. The present cubic cavity represents typically the case of a bulky body where the ratio of volume-to-surface elements is of the same order in number. In this case, the BEM has the clear advantage over the FEM given the relatively large number of volume elements involved. On the other hand, cases involving thin cavities where the ratio of the number of volume to surface elements is small imply

Table I. Comparison between the BEM and the FEM for simple lid-driven three-dimensional cavity flow of a Newtonian fluid

Method	Number of elements	Centre height
BEM	216	0.6815
	486	0.7444
	720	0.7518
	900	0.7593
	1134	0.7630
FEM	64	0.6778
	216	0.7259
	729	0.7452

The table displays the total number of elements and the height of the flow centre in the plane $z = 1$.

a relatively large number of boundary elements. In this case, the BEM loses some of its advantage over the FEM. Second, an accurate comparison and asymptotic storage assessment between the two algorithms is difficult to achieve since the present BEM code and the POLYFLOW™ code may not be constructed in a similar manner. The main reliable information that one may retain from the comparison is the rate at which the CPU grows in each of the two cases.

5.2. Transient rotating flow and non-linear dynamics

Consider now the three-dimensional flow inside the rotating mixer shown in Figure 1. The cubic cavity is of unit side: $-0.5 \le x \le 0.5$, $-0.5 \le y \le 0.5$, $-0.5 \le z \le 0.5$, with the origin coinciding with the centre of the cube. The flow is induced by the rotation of a flat rectangular rotor (vane) initially occupying the region $-0.1 \le x \le 0.1$, $-0.4 \le y \le 0.4$, $-0.4 \le z \le 0.4$ as illustrated in the figure. At $t = 0$, the rotor is set in counter-clockwise motion (around the vertical y-axis) at an angular speed of 1 rev s^{-1}. Since the fluid responds immediately to the motion of the rotor, the flow field is the same for both Newtonian and (linear) viscoelastic fluids. For this reason, viscoelasticity only influences the evolution of stress or traction at the rotor and inner cavity wall, which will now be examined under conditions of complete stick at the boundaries.

The evolution of the traction at the rotor tip, at the point located initially at (0.0, 0.0, 0.4), is first monitored over a period of 2 rev. Both Newtonian fluids ($\lambda_1 = 0$ s) and viscoelastic fluids of the Maxwell type, with $\lambda_1 = 0.1$, 0.2 and 0.3 s, are examined. The evolutions of the traction components t_X and t_Z are shown in Figures 2 and 3 respectively. For a Newtonian fluid, in contrast to viscoelastic fluids, there is a small but non-zero t_X value at $t = 0$ (Figure 2) equal (in magnitude)

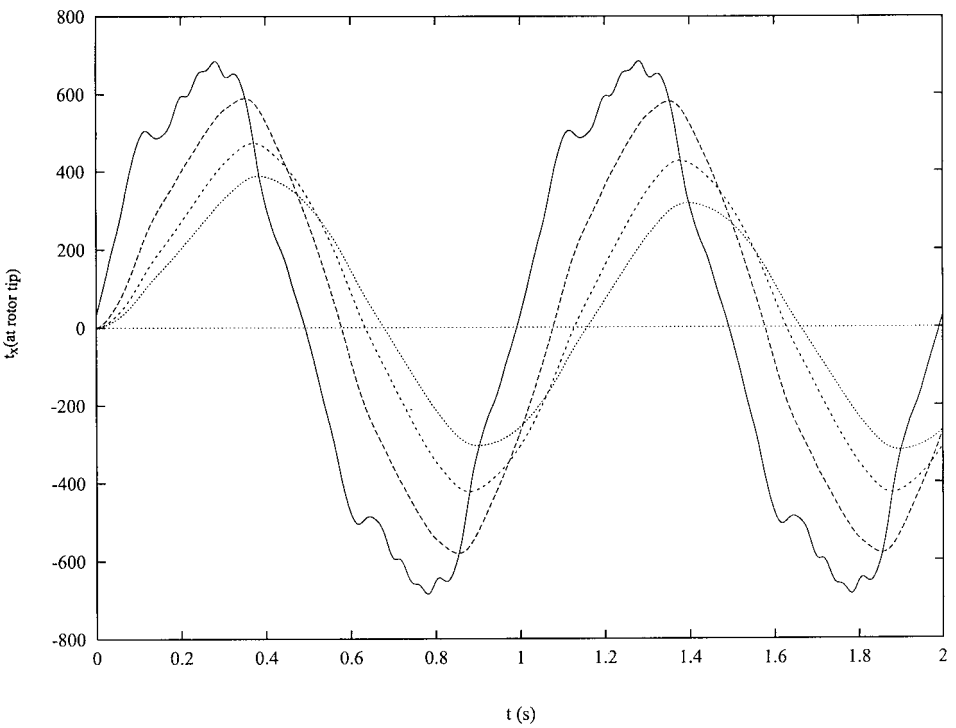

Figure 2. Evolution of t_X at the tip of the rotor, at the point initially located at (0.0, 0.0, 0.4). The long-term signal period is 1 s, corresponding to a full revolution of the rotor. Newtonian fluid (—), Maxwell fluid with $\lambda_1 = 0.1$ s (---), 0.2 s (- - -) and 0.3 s (· · · ·). These curve legends will also be used for Figures 5–7, 10 and 11.

to the slope $u_{X,Z}(0.0, 0.0, 0.4)$. The periodic behaviour in t_X is clearly depicted from Figure 2. For $\lambda_1 > 0$ s, t_X increases from zero, and eventually settles in turn into a similar periodic signal with the same frequency as the Newtonian signal. There is a phase shift relative to the Newtonian signal that increases as the level of fluid elasticity increases. The amplitude of the stress decreases as the fluid becomes more elastic. The figure also shows that any modulation or non-linear behaviour in the time signature tends to disappear as λ_1 increases.

The evolution of t_Z at the same location is shown in Figure 3. In this case, the difference in initial behaviour between Newtonian and viscoelastic flows is more obvious. This difference is most probably due to the effect of the (hydrostatic) pressure since $u_{Z,Z}$ is not expected to be large compared with $u_{X,Z}$ at (0.0, 0.0, 0.4) over a 0.1 gap between the tip of the rotor (at the plane $z = 0.4$) and the opposite cavity side ($z = 0.5$). The component t_Z increases monotonically with time for viscoelastic fluids until periodic behaviour is attained.

Both Figures 2 and 3 reflect clearly a non-linear behaviour in the evolution of the traction. This non-linear character is further evidenced when the long-term phase portrait is examined after transient effects die out. This is depicted from Figure 4, which shows the trajectories in the (t_X, t_Z) plane for Newtonian and viscoelastic fluids. The phase trajectories clearly illustrate the periodic nature of the force signal with a decrease in amplitude as λ_1 increases. More importantly, the non-linear character of the signal decreases gradually for the viscoelastic fluids, until the signal becomes essentially linear for $\lambda_1 = 0.3$ s. The initial growth of the viscoelastic traction, and its approaching the Newtonian limit with a phase shift, are reminiscent of problems in sudden inception of steady state and oscillatory plane and rotating Couette flows [20].

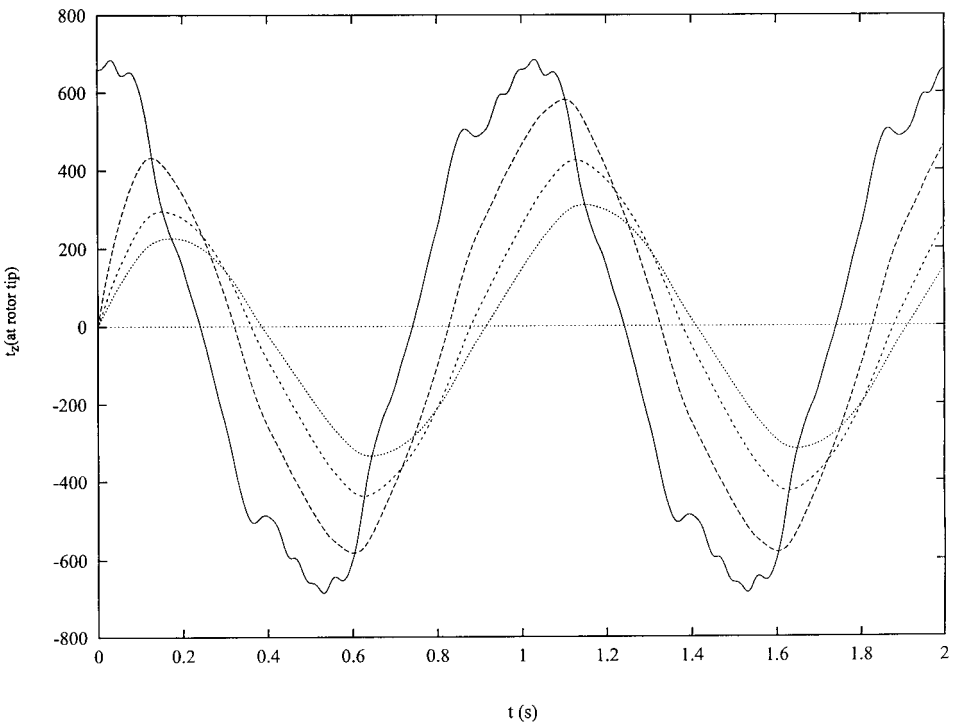

Figure 3. Evolution of t_Z at the tip of the rotor, at the point initially located at (0.0, 0.0, 0.4). The long-term signal period is 1 s, corresponding to a full revolution of the rotor.

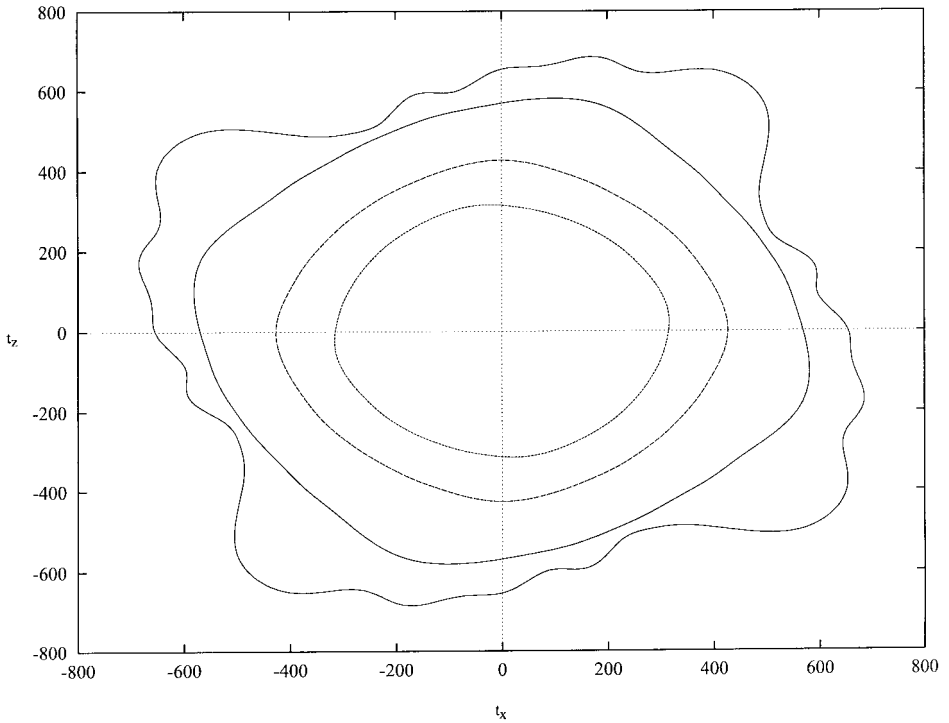

Figure 4. Long-term phase–plane behaviour of the traction components t_X and t_Z at the tip of the rotor, at the point initially located at (0.0, 0.0, 0.4).

From Figures 2 and 3, one may hastily conclude that the evolution of the x and z components of the traction at the tip of the rotor typically represent the overall behaviour of the traction (magnitude) or components in other directions. However, the behaviours of the tangential and normal components hardly resemble those in the figures. From the values of t_X and t_Z, the evolution of the tangential and normal forces, t_t and t_n respectively, are determined. These components are of more physical and practical relevance to mixing. While the behaviour of the Newtonian signature for t_t is similar to that of t_X and t_Z, that of the viscoelastic components, especially the early transients, is drastically different as presented in Figure 5. For $\lambda_1 > 0$ s, there is generally a sharp initial drop in the value of t_t with an undershoot beyond which the force signature settles into periodic motion. As the level of elasticity increase, with λ_1 remaining small, the mean value of oscillation decreases monotonically with λ_1. However, this monotonic response is broken as λ_1 exceeds a critical value. This behaviour is clearly depicted in Figure 5 as the mean value for $\lambda_1 = 0.3$ s is higher than that corresponding to $\lambda_1 = 0.2$ s.

The evolution of t_n reported in Figure 6 also reveals unexpected and interesting dynamics for the same viscoelastic fluids considered above. Unlike t_X and t_Z, the Newtonian normal force is always positive, with a frequency four times larger (see Figures 2 and 3). Typically, for a viscoelastic fluid, t_n increases initially from zero and settles into periodic behaviour with smaller amplitude than for a Newtonian fluid. For $\lambda_1 > 0.1$ s, there is an overshoot before periodic motion sets in. Obviously, this is not related to the overshoot resulting from the non-linear elastic normal stresses (that leads to the well-known Weissenberg rod-climbing

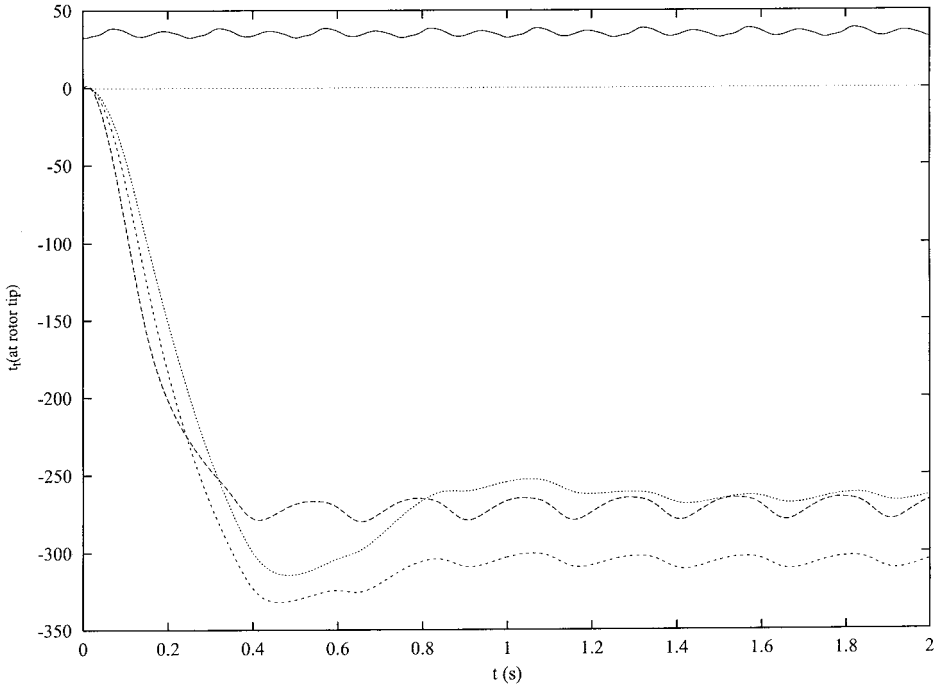

Figure 5. Evolution of the tangential force t_t at the tip of the rotor, at the point initially located at (0.0, 0.0, 0.4). The long-term signal period is 0.5 s, corresponding to half a revolution of the rotor.

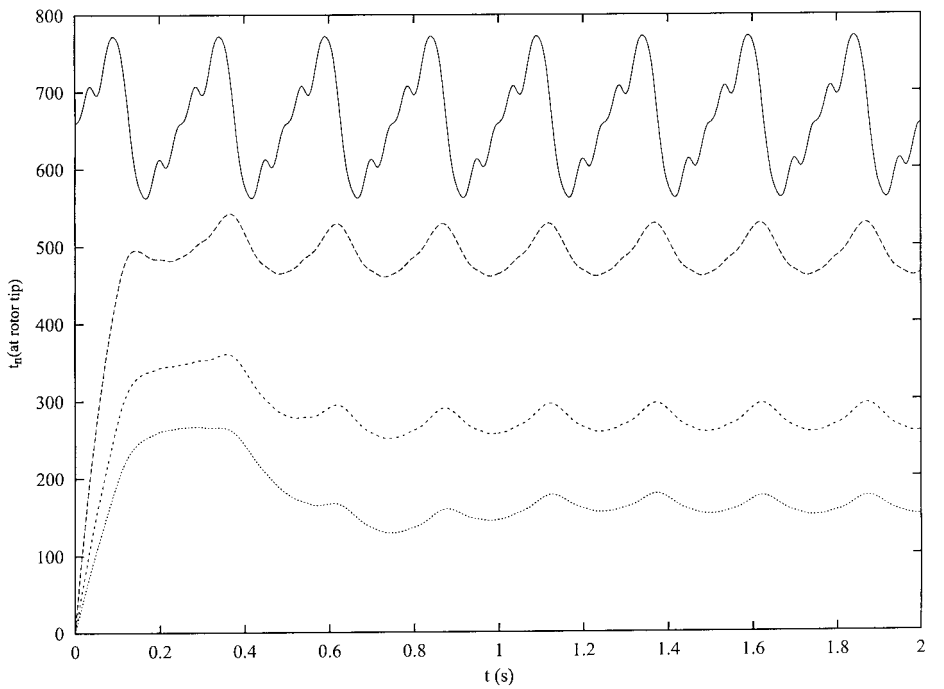

Figure 6. Evolution of the normal force t_n at the tip of the rotor, at the point initially located at (0.0, 0.0, 0.4). The long-term signal period is 0.25 s, corresponding to a quarter revolution of the rotor.

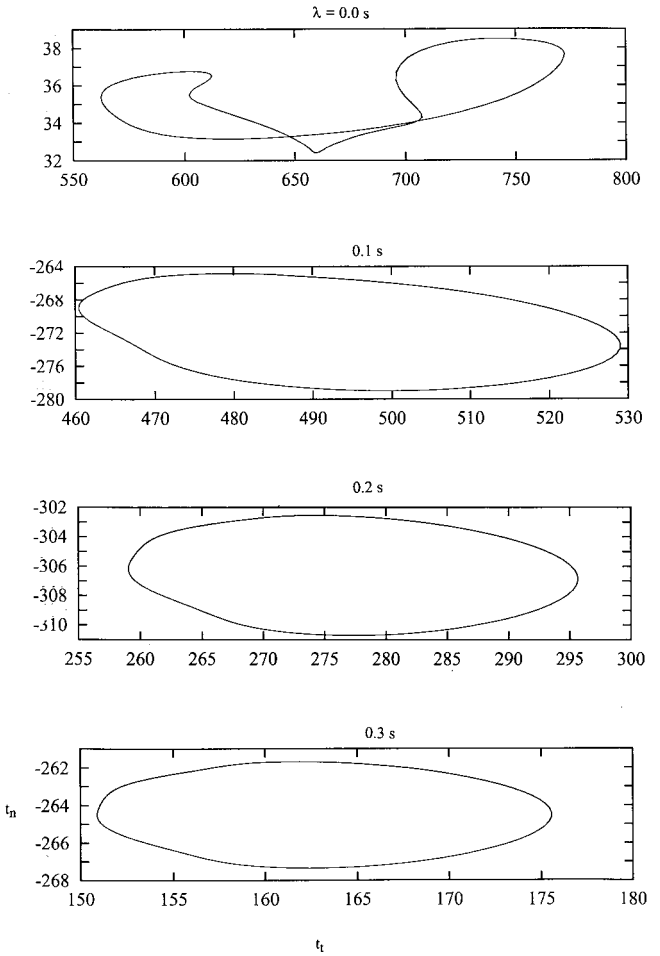

Figure 7. Long-term phase–plane behaviour of the normal and tangential forces t_n and t_t at the tip of the rotor, at the point initially located at (0.0, 0.0, 0.4) for a Maxwell fluid [$0.0 \leq \lambda_1$ (s) ≤ 0.3].

phenomenon) in sudden inception flows [20]. The evolution of the viscoelastic normal traction should thus be interpreted with some caution since the role of the more realistic non-linear normal stresses is not accounted for in the present formulation. Note that, in contrast to the tangential component, the normal traction oscillates around a mean value that decreases monotonically as λ_1 increases.

The long-term phase trajectories in the (t_t, t_n) plane are shown in Figure 7. The Newtonian orbit (Figure 7(a)) is multiply connected, reflecting strong non-linearity and the period doubling (see also Figures 5 and 6). The non-linear character gradually disappears as λ_1 increases from zero (Figure 7(b)–(d)), confirming what has already been established in Figures 5 and 6.

The spatio-temporal behaviour is further examined by considering the corresponding power spectra reported in Figure 8. All power spectra in the figure show very similar frequency distributions despite the different temporal signatures and phase–plane trajectories. They all show the presence of one dominant frequency and its harmonics. There is at least one subharmonic corresponding to half the dominant frequency, confirming the presence of a

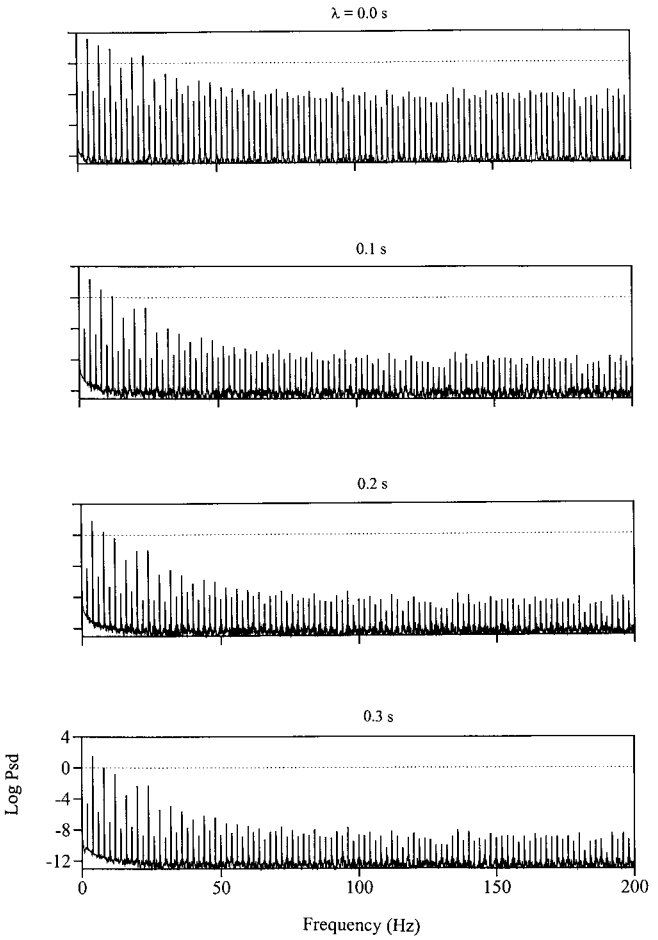

Figure 8. Long-term power–density spectra of the normal force t_n at the tip of the rotor, at the point initially located at (0.0, 0.0, 0.4) for a Maxwell fluid [$0.0 \leq \lambda_1$ (s) ≤ 0.3].

period doubling. The dominant frequency, its harmonics and subharmonics are essentially the same for both Newtonian and viscoelastic fluids. They just diminish in intensity as fluid elasticity increases.

The evolution of the force acting on the outer boundary is also examined, in particular, in the middle of the face $z = 0.5$. The behaviour of the normal force t_Z at the point (0.0, 0.0, 0.5) is reported in Figure 9, which seems to be much more irregular than that of the force at the tip of the rotor. In this case, periodic behaviour sets in almost after 1 rev and is equal to 0.5 s (0.5 rev). The amplitude of the viscoelastic signal is considerably smaller. This is somewhat contrary to what one expects since, the addition of elasticity, in lubrication for instance, tends to increase the normal force. But again, one may have to account for the non-linear normal stresses to deduce the global picture. The evolution of the tangential force t_X at (0.0, 0.0, 0.5) is shown in Figure 10. It is interesting to observe from Figures 9 and 10 that the overall amplitude of t_X is much smaller than that of t_Z and fluctuates less. If the contribution to t_Z stems mainly from the hydrostatic pressure, then Figure 9 shows a strong fluctuation in pressure. Obviously, t_X is always negative as the friction force opposes the (local) motion in the

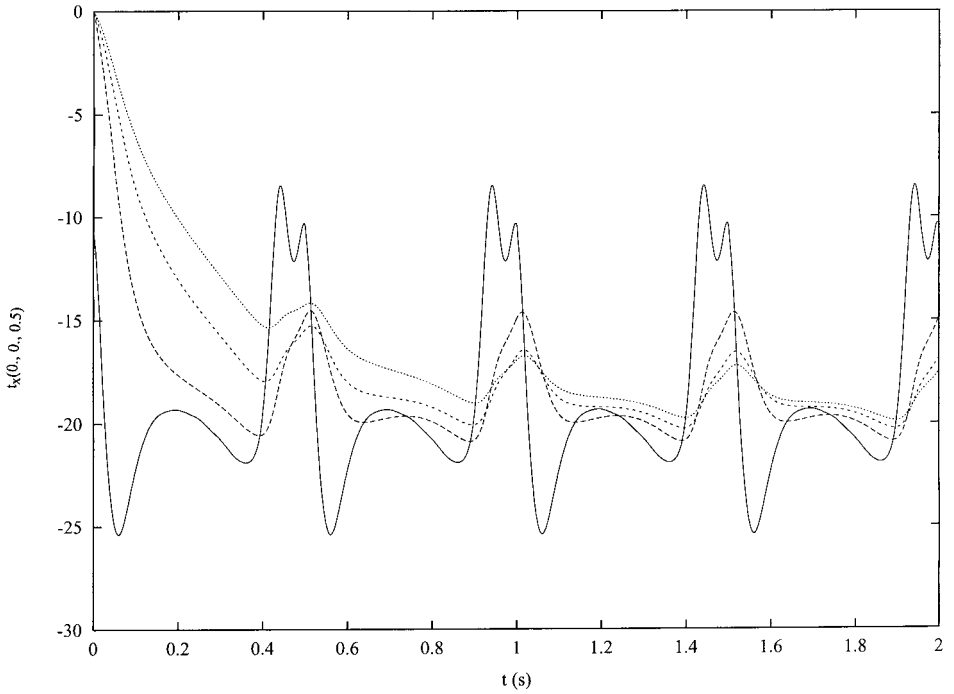

Figure 9. Evolution of the normal force t_Z in the middle of the face $z = 0.5$ at (0.0, 0.0, 0.5). The long-term signal period is 0.5 s, corresponding to half a revolution of the rotor.

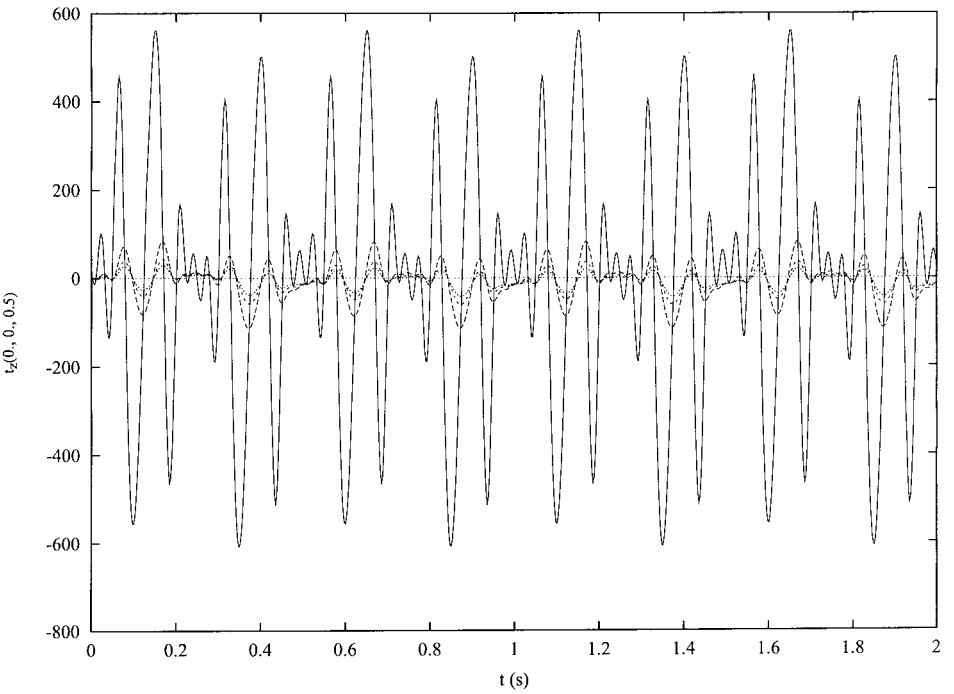

Figure 10. Evolution of the tangential force t_X in the middle of the face $z = 0.5$ at (0.0, 0.0, 0.5). The long-term signal period is 0.5 s, corresponding to half a revolution of the rotor.

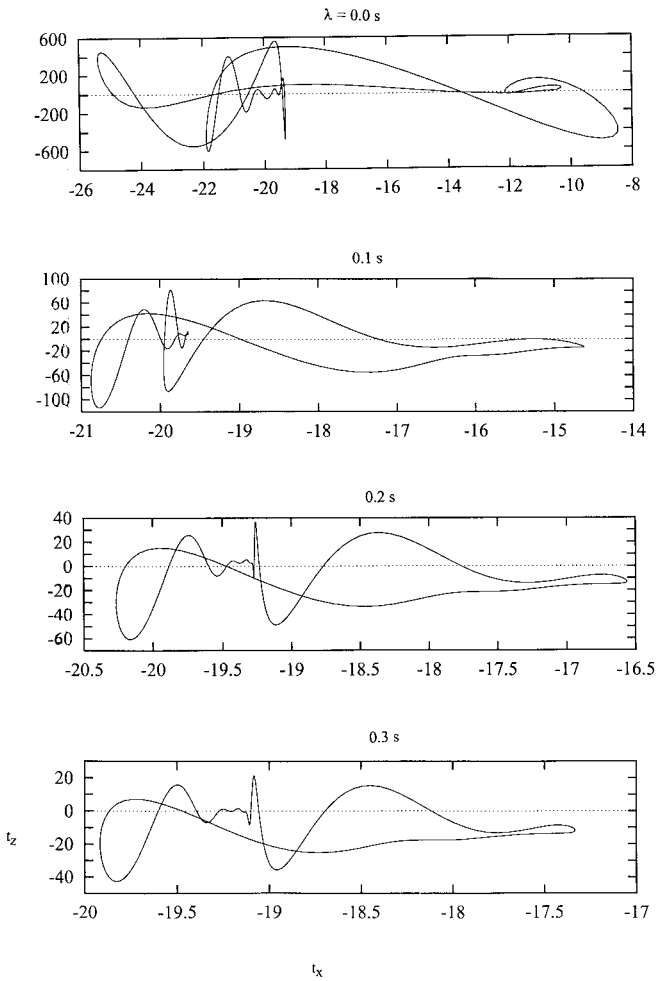

Figure 11. Long-term phase–plane behaviour of the normal and tangential forces t_n and t_t at (0.0, 0.0, 0.5) for a Maxwell fluid [$0.0 \leq \lambda_1$ (s) ≤ 0.3].

positive x-direction. The viscoelastic flow, at least for the range of relaxation times considered, requires more than one full revolution (1 s) to settle into periodic motion. In contrast to the non-linearities in the traction components at the tip of the rotor (Figure 8), the non-linear dynamics for the traction at the cavity face is extremely complicated. This is obvious from the time signatures in Figures 9 and 10, but is also further evidenced in Figure 11, which shows the phase trajectories in the (t_X, t_Z) plane.

6. CONCLUSION

In this study, the applicability of the BEM to cavity mixing is demonstrated for Newtonian and polymer solutions obeying the Jeffreys model. The mixing process is typically unsteady and involves the presence of a moving boundary (vane). The performance of the BEM is assessed against that of the FEM (using POLYFLOW™) for simple lid-driven cavity flow of

a Newtonian fluid. The BEM appears to require less CPU than the FEM for a mesh involving the same number of nodes (internal and external). A direct quantitative comparison is difficult to attain, however, given that the two numerical algorithms are designed differently. What is more conclusive is the rate at which CPU requirement increases with the number of nodes. The rate turned out to grow like $N^{2.36}$ for the FEM and like $N^{1.2}$ for the BEM.

The rotating flow is investigated as induced by the action of a vane inside a rectangular cavity. The influence of viscoelasticity is clearly illustrated in the case of sudden inception in the motion of the vane. The evolution of the tractions at the rotor tip reveals complex dynamics and transient behaviour. While the traction for a Newtonian fluid settles into periodic motion right from the beginning, the traction for a viscoelastic fluid is found to undergo a transient evolution before it reaches periodic behaviour. The viscoelastic signal exhibits generally a phase shift and has an amplitude that decreases as the level of fluid elasticity increases. While the constitutive equations used (for creeping Newtonian fluids and viscoelastic fluids of the Maxwell type) are linear, the response of the traction is highly non-linear.

ACKNOWLEDGMENTS

This work is funded by the Natural Sciences and Engineering Research Council of Canada.

REFERENCES

1. G. de Vahl Davis and G.D. Mallison, 'An evaluation of upwind and central difference approximation by a study of recirculating flow', *Comput. Fluids*, **4**, 29 (1976).
2. R. Pan and A. Acrivos, 'Steady flows in rectangular cavities', *J. Fluid Mech.*, **28**, 643 (1967).
3. R. Schreiber and H.B. Keller, 'Spurious solutions in a driven cavity calculations', *J. Comput. Phys.*, **49**, 165 (1983).
4. R. Peyret and T.D. Taylor, *Computational Methods of Fluid Flow*, Springer, Berlin, 1983.
5. W.L. Chien, H. Rising and J.M. Ottino, 'Laminar mixing and chaotic mixing in several cavity flows', *J. Fluid Mech.*, **170**, 355 (1986).
6. S. Smale, 'Differentiable dynamical systems', *Bull. Am. Math. Soc.*, **73**, 747 (1967).
7. C.W. Leong and J.M. Ottino, 'Experiments on mixing due to chaotic advection in a cavity', *J. Fluid Mech.*, **209**, 463 (1989).
8. A.B. Cortes and J.D. Miller, 'Numerical experiments with the lid-driven cavity flow problem', *Comput. Fluids.*, **23**, 1005 (1994).
9. P.J. Gramann, L. Stradins and T.A. Osswald, 'Flow and heat transfer simulation of the mixing of polymer blends using the boundary element method', *Int. Polym. Proc.*, **8**, 287 (1993).
10. K. Gustafson and K. Halasi, 'Vortex dynamics of cavity flows', *J. Comput. Phys.*, **64**, 279 (1986).
11. C.H. Bruneau and C. Jouron, 'An efficient scheme for solving steady incompressible Navier–Stokes equations', *J. Comput. Phys.*, **89**, 389 (1990).
12. J.W. Goodrich, K. Gustafson and K. Halasi, 'Hopf bifurcation in the driven cavity', *J. Comput. Phys.*, **90**, 219 (1990).
13. J. Shen, 'Hopf bifurcation of the unsteady regularized driven cavity flow', *J. Comput. Phys.*, **95**, 228 (1991).
14. R.E. Khayat, 'Onset of Taylor vortices and chaos in viscoelastic fluids', *Phys. Fluids*, **7**, 2191 (1995).
15. R.E. Khayat, 'Low-dimensional approach to non-linear overstability of purely elastic Taylor-vortex flow', *Phys. Rev. Letts.*, **78**, 4918 (1997).
16. R.E. Khayat, 'Chaos and overstability in the thermal convection of viscoelastic fluids', *J. Non-Newt. Fluid Mech.*, **53**, 227 (1994).
17. R.E. Khayat, 'Non-linear overstability in the thermal convection of viscoelastic fluids', *J. Non-Newt. Fluid Mech.*, **58**, 331–356 (1995).
18. R.E. Khayat, 'Fluid elasticity and transition to chaos in thermal convection', *Phys. Rev. E*, **51**, 380 (1995).
19. R.E. Khayat, 'Chaos in the thermal convection of weakly shear-thinning fluids', *J. Non-Newt. Fluid Mech.*, **63**, 153 (1996).
20. R.B. Bird, R.C. Armstrong and O. Hassager, *Dynamics of Polymeric Liquids*, vol. 1, Wiley, New York, 1987.
21. S.J. Muller, E.S. Shaqfeh and R.G. Larson, 'Experimental study of the onset of oscillatory instability in viscoelastic Taylor–Couette flow', *J. Non-Newt. Fluid Mech.*, **46**, 315 (1993).
22. M.B. Bush and N. Phan-Thien, 'Three-dimensional viscous flows with a free surface: flow out of a long square die', *J. Non-Newt. Fluid Mech.*, **18**, 211 (1985).

23. T. Tran-Cong and N. Phan-Thien, 'Three-dimensional study of extrusion processes by boundary element method. II. Extrusion of a viscoelastic fluid', *Rheol. Acta*, **27**, 639 (1988).
24. C.J. Coleman, 'On the use of boundary integral methods in the analysis of non-Newtonian fluid flow', *J. Non-Newt. Fluid Mech.*, **16**, 347 (1984).
25. M.B. Bush, R.I. Tanner and N. Phan-Thien, 'A boundary element investigation of extrudate swell', *J. Non-Newt. Fluid Mech.*, **18**, 143 (1985).
26. A.J. Nowak, 'Application of the multiple reciprocity method for solving non-linear problems', in L.C. Wrobel, C.A. Brebbia and A.J. Nowak (eds.), *Advanced Computational Methods in Heat Transfer II*, *Vol I: Conduction, Radiation and Phase Change*, Computational Mechanics Publications, Southampton, 1995.
27. A.C. Neves and C.A. Brebbia, 'The multiple reciprocity boundary element method transforming domain integrals to the boundary', *Int. J. Numer. Methods Eng.*, **31**, 709 (1991).
28. P.W. Partridge, C.A. Brebbia and L.C. Wrobel, *The Dual Reciprocity Boundary Element Method*, Computational Mechanic Publications, Southampton, 1992.
29. D. Frayce and R.E. Khayat, 'A dual reciprocity boundary element approach to three-dimensional transient heat conduction as applied to materials processing', *Numer. Heat Transf. A*, **29**, 243 (1996).
30. F.J. Rizzo and D.J. Shippy, 'An application of the corresponding principle of viscoelastic theory', *SIAM J. Appl. Math.*, **21**, 321 (1971).
31. T. Kusama and Y. Mitsui, 'Boundary element method applied to linear viscoelastic analysis', *Appl. Math. Model.*, **6**, 285 (1982).
32. R.M. Christensen, *Theory of Viscoelasticity*, 2nd edn., Pergamon, Oxford, 1982.
33. D.R. Bland, *Theory of Linear Viscoelasticity*, Pergamon, Oxford, 1960.
34. B. Gross, *Mathematical Structure of the Theory of Viscoelasticity*, Hermann, Paris, 1968.
35. W.T. Read, 'Stress analysis for compressible viscoelastic materials', *J. Appl. Phys.*, **21**, 671 (1950).
36. R. Sips, 'General theory of deformation of viscoelastic substances', *J. Ploym. Sci.*, **9**, 191 (1951).
37. M.A. Brull, 'A structural theory incorporating the effect of time-dependent elasticity', *Proc. 1st Midwestern Conference Solid Mechanics*, 1953, p. 141.
38. E.H. Lee, 'Stress analysis in viscoelastic bodies', *Q. Appl. Math.*, **13**, 183 (1955).
39. C. Pozrikidis, *Boundary Integral and Singularity Methods for Linearized Viscous Flow*, Cambridge University Press, Cambridge, 1992.
40. C.A. Brebbia and J. Domingez, *Boundary Element: An Introductory Course*, Computational Mechanic Publications, Southampton, 1992.
41. P.K. Kythe, *An Introduction to Boundary Element Methods*, CRC Press, Boca Raton, FL, 1995.
42. T.A. Cruse, 'Numerical simulation in three dimensional elastostatics', *Int. J. Solids Struct.*, **5**, 1259 (1969).

